Chemical Engineering Journal 157 (2010) 263–269

Contents lists available at ScienceDirect

Chemical Engineering Journal

journal homepage: www.elsevier.com/locate/cej

La^{3+} and Zr^{4+} co-doped anatase nano TiO_2 by sol-microwave method

Abdollah Fallah Shojaie*, Mohammad Hassan Loghmani

Department of Chemistry, Faculty of Science, University of Guilan, P.O. Box 1914, Rasht, Iran

ARTICLE INFO

Article history:
Received 1 September 2009
Received in revised form
12 December 2009
Accepted 16 December 2009

Keywords:
Microwave
Nano TiO_2
co-doped
Lanthanum
Zirconium
4-Nitrophenol

ABSTRACT

Anatase nano TiO_2 powders were prepared by two different methods. One is the sol-microwave method and the other is oil-bath condition synthesis. A microwave oven (800 W) was used as the microwave source. Under 2.45 GHz microwave irradiation, titanium tetra-isopropoxide (TIP) was quickly hydrolyzed and anatase TiO_2 was formed in a short time (<4 min). In addition, a simple sol to gel conversion route has been followed for the preparation of anatase phase at 100 °C under oil-bath condition. The materials characterized by XRD, Raman, SEM-EDX, TEM, FT-IR and UV–vis techniques. XRD and Raman spectroscopy confirmed both pure and co-doped nano TiO_2 have a high degree of crystallinity and existence of fully anatase phase at 500 °C. In the microwave method, XRD and TEM results revealed that the particle size of co-doped nano TiO_2 is smaller than pure nano TiO_2. The photocatalytic activity was tested on the degradation of 4-nitrophenol (4-NP). The nano TiO_2 samples prepared by microwave method were more effective than oil- bath samples.

1. Introduction

TiO_2 has been widely used and investigated owing to its inexpensiveness, strong oxidizing power, non-toxicity and long-term photostability. There are three crystalline polymorphs of titania; anatase, brookite and rutile. Among these polymorphs, anatase is important phase as it attracts more attention for its use as pigments [1], gas sensors [2], catalysts [3], etc. Due to its semiconducting activity, TiO_2 is used as photocatalysts [4] in environmental related problems of pollution control. The optical, electrical and catalytic properties of semiconductors strongly depend on the crystallinity, crystal phase, morphology and the size of the particles. Among the various polymorphs listed above, anatase is found to be photocatalytically more active than the other two [5]. Also, smaller particle size exhibits better photocatalytic activity because of its high surface area [6]. The high rate of electron–hole recombination on TiO_2 particles results in a low efficiency of photocatalysis. For the purpose of overcoming these limitations of TiO_2 as a photocatalyst, numerous studies have been recently performed to enhance electron–hole separation. These studies include doping metal ions into the TiO_2 lattice [7], dye photosensitization on the TiO_2 surface [8], and deposition of noble metals [9]. A number of methods have been used to prepare TiO_2 nanoparticles, such as chemical precipitation [10], microemulsion-mediated hydrothermal [11], hydrothermal crystallization [12–14], sol–gel [15], etc. In sol–gel processes, TiO_2 is usually prepared by the reactions of hydrolysis and polycondensation of titanium alkoxides, Ti $(OR)_n$ to form oxopolymers which are then transformed into an oxide network. To control the hydrolysis process in order to obtain homogeneous titanium oxide networks, some of the chelating reagents such as diol, carboxylic acid, or diketonate compounds are added [12]. The condensation is usually accomplished by gelization and calcination. Condensation pulls together the constitute particles of the gel into a compact mass, thus building up the metal oxide crystal. Microwave-assisted route is one of novel methods and is a very rapidly developing area of research. Compared with conventional methods, microwave synthesis requires very short reaction time, and is capable of producing small particles with a narrow particle size distribution and high purity. There are several reports in the literature of TiO_2 powder preparation by microwave processing. Ramakrishnan synthesized titania ceramic powders from TIP in methanol under microwave irradiation [16]. Aylloïn et al. prepared anatase TiO_2 powder from a fluorine-complexed titanium aqueous solution using microwave irradiation [17]. Also, Komarneni et al. reported microwave-hydrothermal synthesis of titanium dioxide under various reaction conditions [18]. In this study, microwave process was employed following the sol step to prepare the La–Zr–TiO_2 nanoparticles. The hydrolysis of titanium precursors is often performed in acid or alkaline condition. Acid is favorable to hydrolysis reaction, while alkaline is prone to polycondensation reaction. Usually, fast hydrolysis and slow condensation favors the formation of small TiO_2 particles [19]. Thus, the preparation of nano TiO_2 was carried out in the presence of acetic acid. We have also provided the experimental results under no microwave irradiation. For this purpose, sol to gel conversion was carried out under oil-bath condition at 100 °C.

* Corresponding author.
E-mail address: a.f.shojaie@guilan.ac.ir (A.F. Shojaie).

1385-8947/$ – see front matter © 2009 Elsevier B.V. All rights reserved.
doi:10.1016/j.cej.2009.12.025

2. Experimental

2.1. Materials and methods

All the chemicals were obtained from Merck and used as such without further purification.

2.1.1. Sol-microwave method

The reagents employed were titanium (IV) tetra-isopropoxide (TIP), as a TiO_2 source; glacial acetic acid, as a catalyst; $La(NO_3)_3{\cdot}6H_2O$ and $ZrCl_4$, as dopant; citric acid, as a chelating agent; poly ethylene glycol (PEG1000), as a binder reagent; isopropanol (is-prOH), as a solvent and deionized water as a hydrolysis agent. First, anatase TiO_2 nano particles were prepared by means of sol-microwave method. In this method, TIP was initially mixed with is-prOH. To this mixture appropriate amount of citric acid with PEG was added under constant stirring. Then glacial acetic acid was added in it, such that the molar ratio of TIP:acetic acid:is-prOH:citric acid was 1:10:2:0.02. Next, to this solution; a mixture of deionized water and is-prOH (water and is-prOH was in 20:1 molar ratios) was added by drop using a burette. The solution was stirred for 30 min to get a yellow transparent sol. Finally, the sol was placed under microwave (Galanz, 2.45 GHz, 800 W) irradiation (40% power) for 4 min. The white gel product was filtered, washed with distilled water and dried in oven for several hours. It was then calcined at 500 °C in air for 5 h at a ramp rate of 5 °C/min. To prepare La–Zr co-doped anatase nano particles, the above procedure was repeated, including $La(NO_3)_3{\cdot}6H_2O$ (0.4 mol%) and $ZrCl_4$(0.4 mol%) prior to the drop-wise addition of water/is-prOH solution.

2.1.2. Oil-bath method

In this method, the TiO_2 sol was also prepared with above (Section 2.1.1) procedure. Then TiO_2 sol converted to gel by heating under oil-bath condition at 100° C for 30 min. Next, in order to investigate the calcination effect in morphology and size, the sample was heated in furnace at 500° C in air for 5 h at a ramp rate of 5 °C/min. Throughout this work, a set of abbreviations is used: MW, MW1, MW2, OB1 and OB2. The MW refers to microwave used to form the TiO_2 sample, OB to the oil-bath condition, "1" to the un-calcined samples and "2" to the calcined samples.

2.2. Photodegradation of 4-nitrophenol

The photocatalytic activity was tested on the degradation of 4-nitrophenol (4-NP). The degradation intermediates were not determined. The light was provided by a 400 W high pressure Hg lamp without filter which was placed vertically in the reactor. The temperature of photodegradation system was adjusted by a water bath in which heating or cooling water recirculated through the jacket of the beaker. Prior to illumination, the reaction suspension was stirred continuously in dark for 15 min to ensure adsorption/desorption equilibrium. The suspension was magnetically stirred and bubbled with pure oxygen gas. After filtration, the concentration of 4-NP was determined by measuring its absorption by means of a RAYLEIGH (UV-1800) ultraviolet-visible (UV–vis) scanning spectrometer.

2.3. Characterization methods

X-ray diffraction (XRD) patterns were recorded by a D8 Bruker Advanced, X-ray diffractometer using Cu Kα radiation (λ = 1.54 Å). The patterns were collected in the range 20–80° 2θ and continuous scan mode. The compositional analysis was done by energy dispersive X-ray. Scanning electron microscopy (SEM) images were obtained on Philips XL30 equipped with an energy dispersive X-ray spectroscopy. Transmission electron microscope (TEM) images were obtained on a Philips CM10 transmission electron microscope with an accelerating voltage of 100 kV. Fourier transform infrared (FT-IR) spectra were recorded on SHIMADZU 8800 spectrophotometer in KBr pellets. The electronic spectrum of the nano doped TiO_2 was taken on a RAYLEIGH (UV-1800) ultraviolet-visible (UV–vis) scanning spectrometer. Raman spectra were recorded on Almega Thermo Nicolet dispersive spectrometer. An Nd:Y laser was used as an excitation source with 532 nm wavelength.

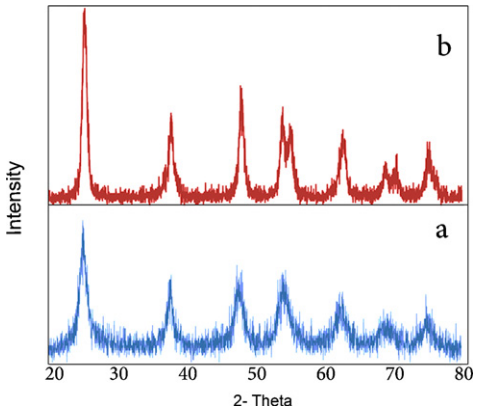

Fig. 1. XRD patterns of TiO_2 synthesized through the oil-bath method: (a) before calcination and (b) after calcination.

3. Results and discussion

3.1. X-ray diffraction (XRD) studies

The XRD patterns (Fig. 1), of the oil-bath samples, OB1 and OB2, match perfectly with the JCPDS card no. 21-1272 and no. 21-1271, respectively. Therefore, all the sharp peaks could be indexed as anatase phase. The results indicated that there was no significant change in the phase composition of either un-calcined or calcined nano TiO_2. However, the intensity of the diffraction peaks of the nano TiO_2 increased after calcination. The XRD patterns of microwave-assisted samples are shown in Fig. 2. They are also basically in agreement with the JCPDS card no. 21-1272. The rutile phase appeared in XRD pattern before calcination. It appears

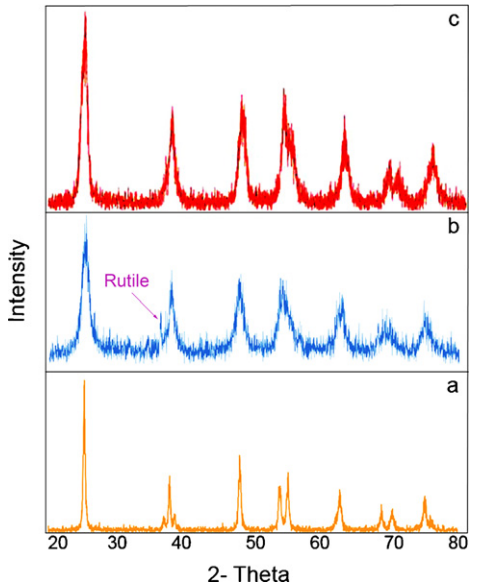

Fig. 2. XRD patterns of TiO_2 prepared through the sol-microwave method: (a) pure (MW), (b) un-calcined co-doped TiO_2 (MW1) and (c) calcined co-doped TiO_2 (MW2).

Table 1
Details and size of the all samples.

Sample details	Method	Size (nm):	
		XRD[a]	TEM[b]
MW	Sol-microwave, calcined at 500 °C, pure TiO_2	12	25
MW1	Sol-microwave, un-calcined, co-doped TiO_2	6	5
MW2	Sol-microwave, calcined at 500 °C, co-doped TiO_2	8	15
OB1	Oil-bath synthesis, un-calcined, co-doped TiO_2	7	10
OB2	Oil-bath synthesis, calcined at 500 °C, co-doped TiO_2	10	15

[a] Estimated by means of the Scherrers equation from broadening of (1 0 1) anatase reflection.
[b] Estimated by direct measuring the particle size on the TEM images.

around $2\theta = 36.27^\circ$. In addition, Fig. 2 displays that, characteristic peaks broadened when the ions doped into TiO_2. However, no peaks from any else impurities were observed, which indicates the high purity of the obtained La–Zr co-doped. The sharp diffraction peaks manifest that the obtained TiO_2 have high crystallinity. Using the Scherrer equation, the crystallite diameters of all fives samples were calculated. The details of the samples are summarized in Table 1. The ionic radius is the most important condition, which can strongly influence the ability of the dopant to enter into TiO_2 crystal lattice. If the ionic radius of the doping metal ions matches those of the lattice metal ion in oxides, the doping metal ion will substitute itself for the lattice in the doping reactive process (substitutional mode). While if the ionic radius of the dopant is much bigger or smaller than that of Ti^{4+}, the dopant substituting for TiO_2 crystal lattice ions must result into crystal lattice distortion (CLD). Modification of the surface state of the catalyst might be causing effective separation of electron–hole pairs (e^-h^+). In fact the ionic radius of La^{3+} (0.115 nm) is bigger than that of Ti^{4+} (0.068 nm). Therefore, it is difficult for La^{3+} to really enter into the lattice of TiO_2. But Since the electronegativity and the ionic radius of Zr^{4+} ion (1.2, 0.072 nm) are closer to Ti^{4+} ion, it is expected Zr^{4+} ions will replace lattice Ti^{4+} ions and thus occupy lattice Ti^{4+} positions in the doping reactive process and it can either isomorphously substituted or interstitially introduced into the matrix of TiO_2 to produce oxygen vacancies which accelerate the transition and nanocrystallite growth of anatase TiO_2. In addition, La–Zr doped TiO_2 (Fig. 2(c)) did not give any peak corresponding to ZrO_2 or La_2O_3, possibly demonstrating that La^{3+} and Zr^{4+} were dispersed uniformly onto TiO_2 nanoparticles as the form of small cluster La_2O_3 or ZrO_2. This is due to the formation of nanosize particles in the range undetectable by XRD. If Ti^{4+} replaces La^{3+}, a charge imbalance would occur. Therefore, both formation of Ti –O–La bond and charge imbalance might affect the photocatalytic activity of doped TiO_2 catalyst [20]. The charge imbalance must be satiated, so more hydroxide ions would be adsorbed onto the surface for charge balance. These hydroxide ions on the surface can accept holes generated by light irradiation to form hydroxyl radicals, which oxidize adsorbed substrates. Therefore, the photoinduced charge carriers recombination can be suppressed. Xu et al. [21] reported that when the concentration of dopant ions increases, the surface barrier becomes higher, and the space charge region becomes narrower, the electron–hole pairs within the region are efficiently separated by the large electric field before recombination. The formation of Ti–O–Zr or Ti–O–La inhibits the transition of TiO_2 phase and blocks the Ti–O species at the interface with TiO_2 domains stabilizing them, thus preventing the agglomeration of TiO_2 nanoparticles and thus preventing the rutile growth [22].

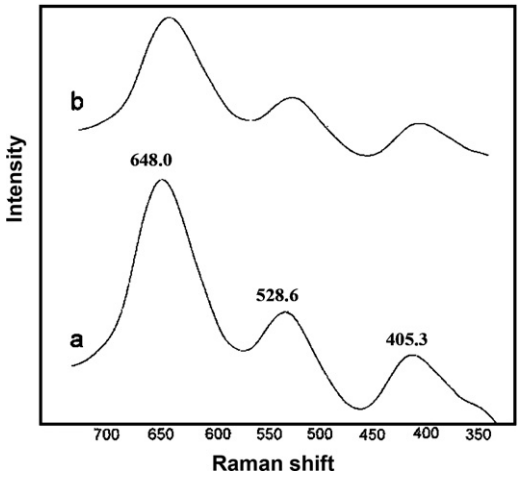

Fig. 3. Raman spectra of TiO_2 (a) pure and (b) La–Zr co-doped prepared through the sol-microwave method.

Hence, the entry of Zr^{4+} and La^{3+}in the TiO_2 lattices suppresses the particle growth and consequently increases the band gap values of TiO_2, which minimizes the electron–hole recombination during the photocatalytic degradation.

3.2. Raman spectroscopy

The Raman spectra of the pure TiO_2, MW, and co-doped TiO_2, MW2, obtained after the 500 °C calcination are presented in Fig. 3(a) and (b), respectively. Optical Raman spectroscopy is a powerful tool in the study of TiO_2 for its high sensitivity to the microstructure. The spectra consist of three peaks. The bands at 405.3 and 528.6 cm^{-1} are assigned to B_{1g} and that at 648 cm^{-1} is assigned to E_g mode of vibrations of anatase titania phase [23,24]. Absence of Raman bands (235, 447 and 612 cm^{-1}) corresponding to rutile phase of titania, again confirms the phase purity of our sample [25]. There is also a significant decrease in the intensity of the Raman bands with doping La and Zr ions. Interestingly, the Raman spectrum in the present work did not show any trace of ZrO_2 or La_2O_3, implying that the amount of ZrO_2 and La_2O_3 were too low to be checked out. These results indicate that Zr or La does not exist as a separate crystalline oxide phase and must be incorporated in the crystal lattice of TiO_2. Thus the Raman spectroscopy data in conjunction with XRD results establish the incorporation of Zr and La in the lattice of TiO_2.

3.3. SEM and TEM micrographs

SEM micrographs of all five samples are shown in Fig. 4. It is observed that nano TiO_2 are in pseudospherical shapes. All samples present strong agglomeration when seen by SEM; the morphology and particle size of them cannot be resolved using this technique. The EDX data of co-doped TiO_2 (MW2) is shown in Fig. 4(d). There are La and Zr peaks in the EDX pattern that this observation gave convincing evidence for the presence of zirconium and lanthanum on the surface of TiO_2. Fig. 5 depicts transmission electron micrographs of all samples. TEM is a useful technique for

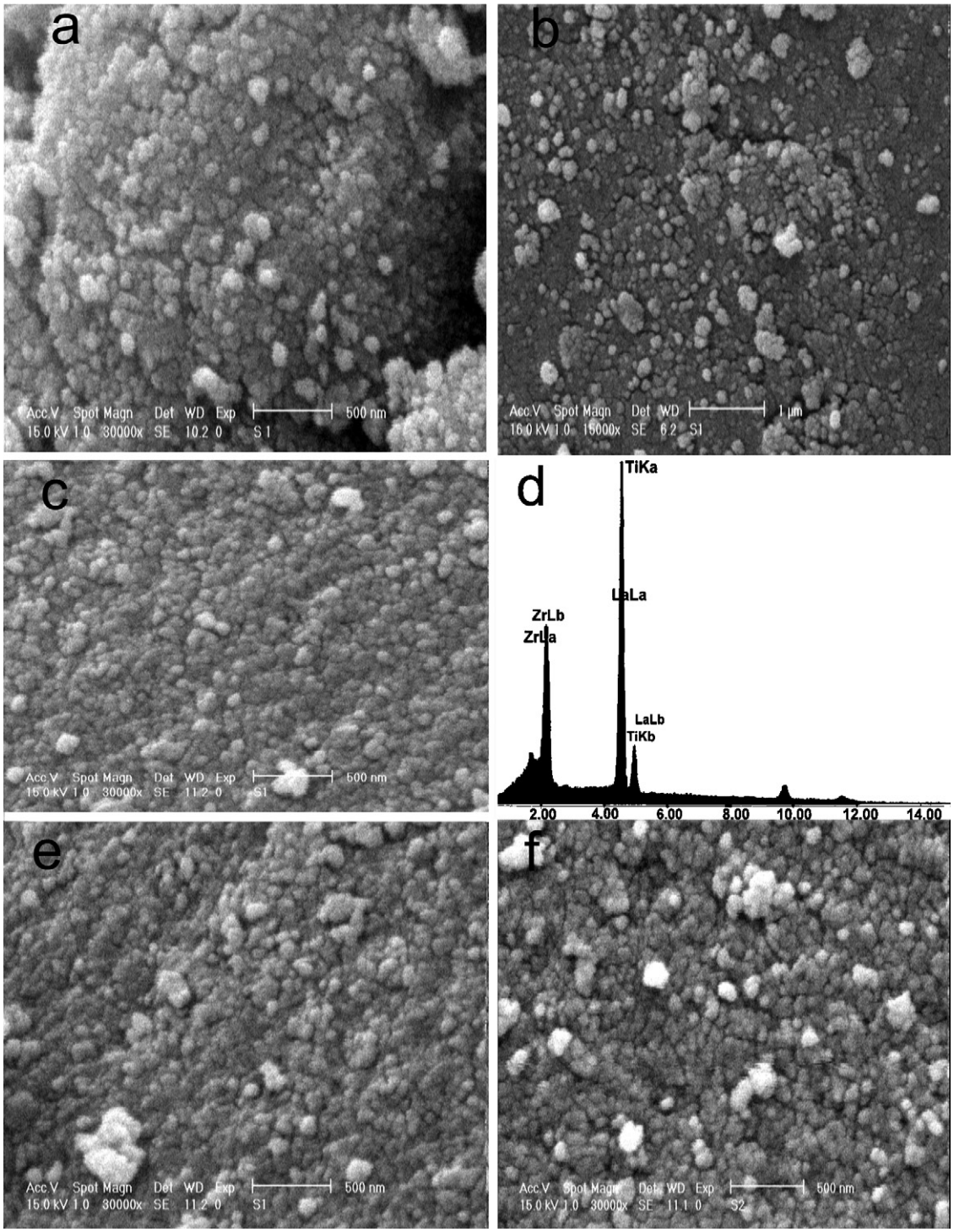

Fig. 4. (a) SEM image of MW, (b) SEM image of MW1, (c) SEM image of MW2, (d) EDX pattern of MW2, (e) SEM image of OB1 and (f) SEM image of OB2.

the analysis of the size and shape of ultrafine particles. The shape of the microwave-assisted co-doped TiO_2, MW1, was observed as nanocluster (Fig. 5(a)) with average size of ~5 nm is consistent with the XRD results. After calcination, MW2, the micrograph (Fig. 5(b)) exhibits co-doped nanocrystalline TiO_2 with average size of ~15 nm. Whereas, Fig. 5(c) shows the nanocrystallites of pure TiO_2, MW, with average size of ~25 nm. The samples prepared under oil-bath condition vary in shape and size. Before calcination, OB1 (Fig. 5(d)), rice-like particles sized 10 nm are observed. After calcination, OB2, the TEM image (Fig. 5(e)) exhibits polygon nanoparticles with a size of about 15 nm. Indeed, it is demonstrated that Zr and La dopant could inhibit the increase of TiO_2 particle size. Therefore, this result may be attributed to the presence of dopant component in the TiO_2 framework. The particle size distribution obtained from the analysis of TEM images is also shown in Fig. 6. Pure nanocrystalline TiO_2, MW, were largely distributed around 14–37 nm. On the other hand, the co-doped microwave-assisted nanocrystalline TiO_2, MW2, was sharply distributed around 9–23 nm. In addition, OB2, was distributed around 7–30 nm.

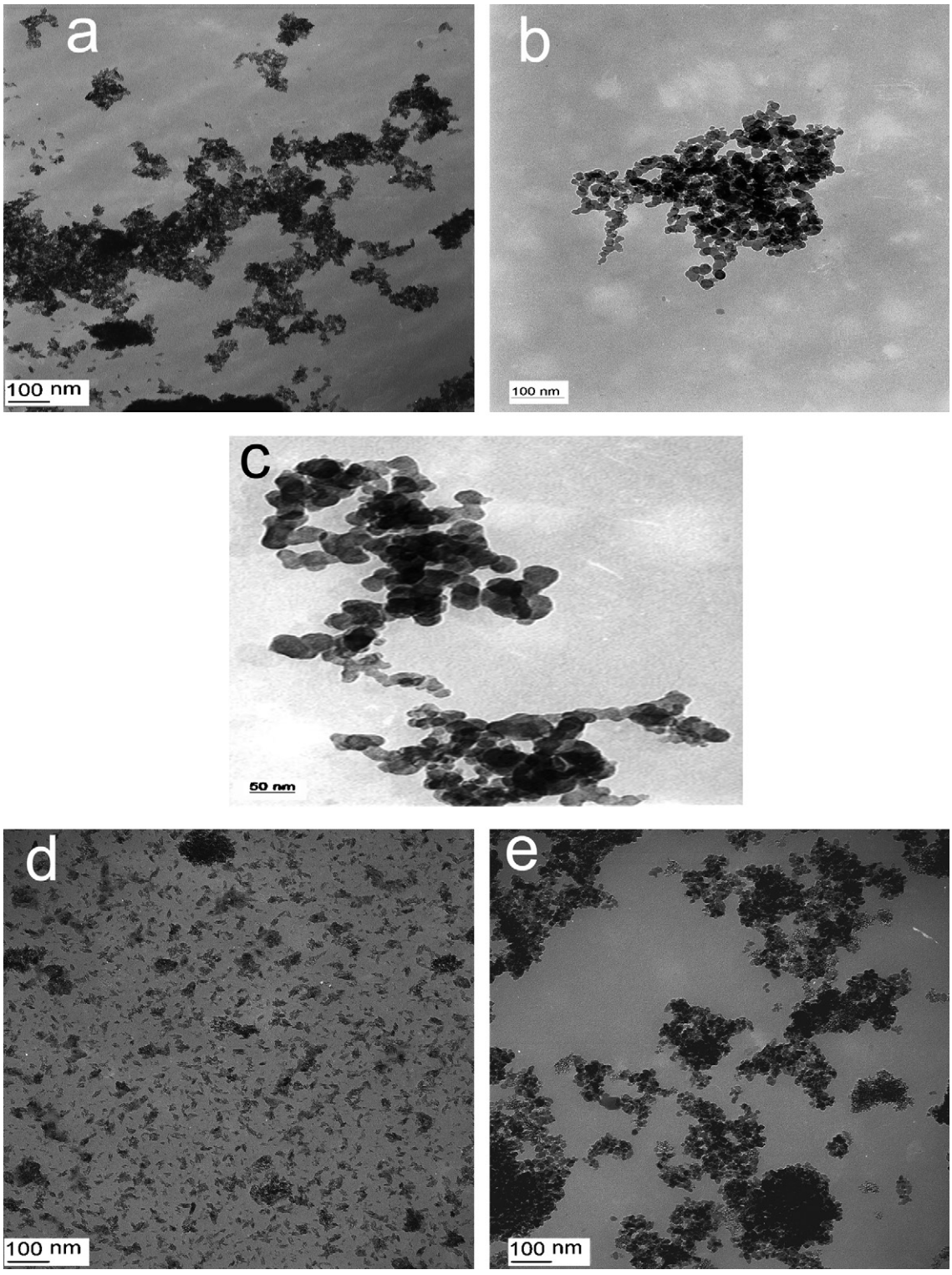

Fig. 5. TEM images of (a) MW1, (b) MW2, (c) MW, (d) OB1 and (e) OB2.

3.4. UV-visible spectrum

UV–vis absorption spectra of pure, microwave-assisted and oil-bath condition samples are shown in Fig. 7 to examine the effect of doped transition metals on the light absorbance in ultraviolet and visible light regions. In ultraviolet light regions, which are shorter than 340 nm, pure nano TiO_2 whose band gap energy equivalent to around 340 nm (3.6 eV) shows the highest absorbance due to charge-transfer from the valence band (mainly formed by 2p orbitals of the oxide anions) to the conduction band (mainly formed by 3d t_2g orbitals of the Ti^{4+} cations) [26]. When La^{3+} and Zr^{4+} were doped, however, the spectra moved toward a shorter wavelength region compared to that of pure TiO_2. Hence, there is sufficient decrease in the particle size and increase in the band gap value due to La and Zr doping. Furthermore, zirconium is in the +4 oxidation state and the valence band of TiO_2 consists of only the O (2p)

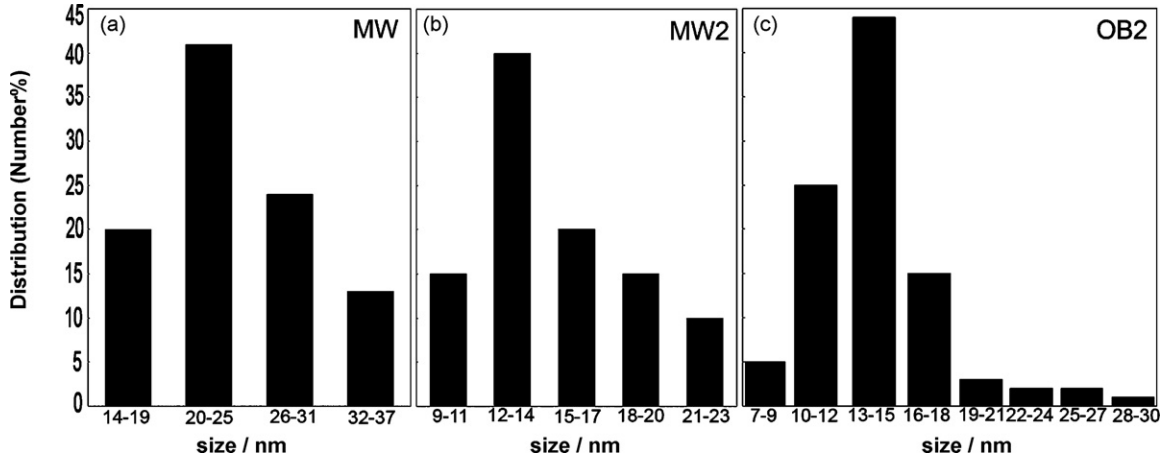

Fig. 6. Particle distribution of synthesized samples: (a) pure, (b) La–Zr–TiO_2 synthesized through the sol-microwave method and (c) La–Zr–TiO_2 prepared through the oil-bath method.

band. This O (2p) band is stabilized more on Zr^{4+} doping since it is more electropositive than Ti^{4+}. Hence, there is an increase in the band gap of TiO_2 [27].

3.5. FT- IR studies

The FT-IR spectra of all five samples are depicted in Fig. 8. The un-calcined samples, MW1 and OB1, show peaks corresponding to the stretching vibrations of O–H and bending vibrations of adsorbed water molecules around 3300–3400 and 1620–1630 cm^{-1}, respectively. In addition, the C–H bending (1360–1470 cm^{-1}) are also well defined. The low intensity of these peaks after calcination is indicating the removal of large portion of adsorbed water and organic molecules from TiO_2. The vibration modes of anatase skeletal O–Ti–O bonds were observed in the range of 500–900 cm^{-1} [28].

3.6. Kinetics of 4-NP disappearance

Fig. 9 shows the kinetics of the disappearance of 4-NP from an initial concentration of 10 ppm under three conditions. There was no considerable reaction rate when the irradiation was carried out in the absence of TiO_2. In non-irradiated suspensions, there was a slight loss, ca. 5%, due to adsorption onto TiO_2 particles. However, in the presence of TiO_2, a rapid degradation of 4-NP occurred by irradiation. The remaining concentration change amounts to 6% after irradiating for 115 min. Indeed, metal ion acts as an effective separation center for electrons and holes. The photogenerated charge carriers can be transferred to different surface sites where they will react with adsorbed 4-NP and enhance photocatalytic activity. Thus, the photoexcited electrons in the conduction band of TiO_2 can be accepted by La^{3+} and Zr^{4+}.

3.7. Effect of mass of TiO_2

The variation in degradation percent of 4-NP against the concentration of TiO_2 was determined (Fig. 10) over the range 0–50 mg. As expected, the degradation was found to increase with the increasing concentration of TiO_2 and approaching a certain point at high concentration, and then begins to decrease slowly. Maximum degradation was obtained at a TiO_2 concentration of 35 mg. This limiting value mainly results from following two factors: (a) aggregation of TiO_2 particles at high concentrations, causing a decrease in the number of surface active sites, and (b) increase in opacity and

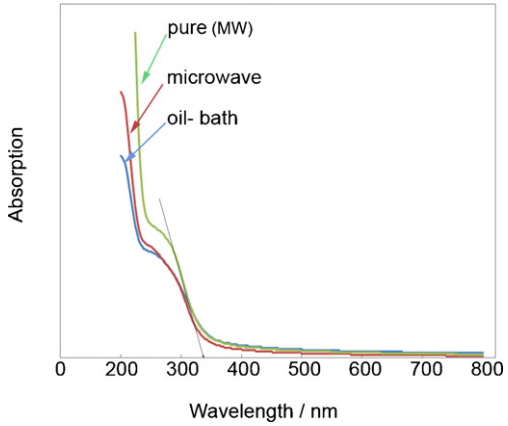

Fig. 7. UV–vis spectra of synthesized pureTiO_2 and co-doped TiO_2.

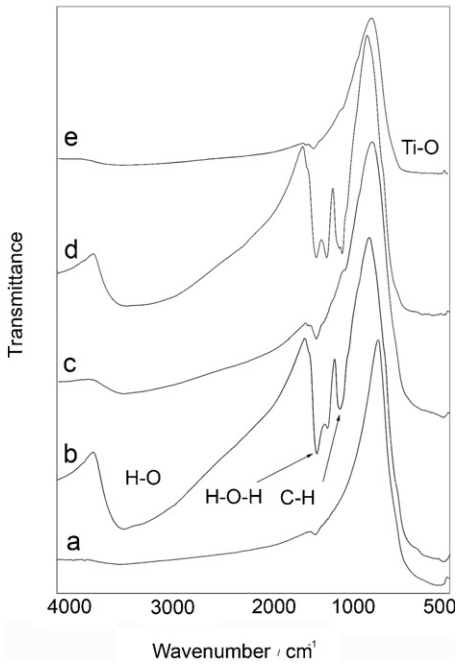

Fig. 8. FT-IR spectra of synthesized TiO_2 and La–Zr co-doped TiO_2: (a) pure (MW), (b) un-calcined La–Zr–TiO_2 (MW1), (c) calcined La–Zr–TiO_2 (MW2), (d) un-calcined co-doped TiO_2 (OB1) and (e) calcined co-doped TiO_2 (OB2).

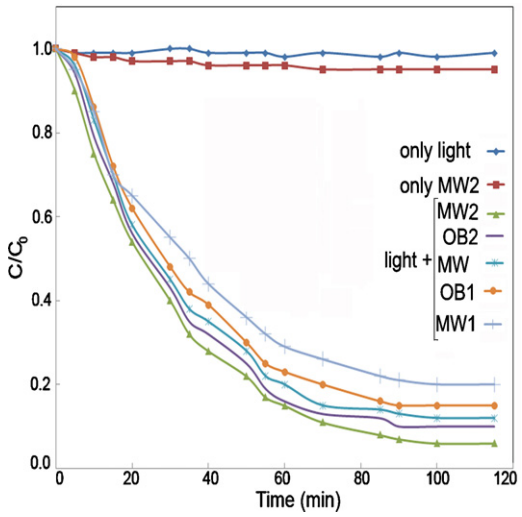

Fig. 9. Photocatalytic disappearance of 4-NP (initial concentration of the 4-NP = 10 ppm, photocatalyst = 35 mg).

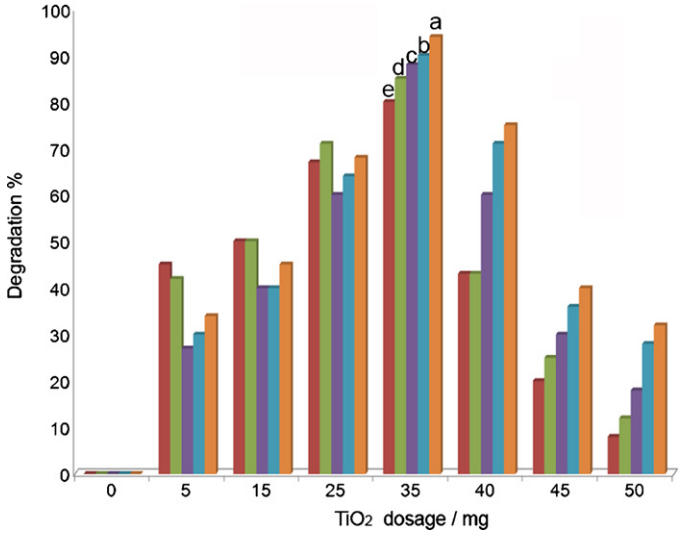

Fig. 10. Effect of TiO_2 dosage on the degradation (initial concentration of the 4-NP = 10 ppm): (a) MW2, (b) OB2, (c) MW, (d) OB1 and (e) MW1.

light scattering of TiO_2 particles at high concentration leading to a decrease in the passage of irradiation through the sample.

4. Conclusions

This study showed that TiO_2 particles with the anatase structure of nano size could be synthesized by the sol-microwave and oil-bath method, which are reproducible and reliable methods. In the microwave method, the particle size of co-doped nano TiO_2 is smaller than that of pure nano TiO_2. In the oil-bath method, anatase nano TiO_2 were prepared at 100 °C. The results of degradation reaction emphasize the role of La and Zr in enhancing photocatalytic activity of TiO_2 under UV light irradiation. The nano TiO_2 prepared by microwave method were more effective than oil-bath sample. The significant enhancement of the photocatalytic activity of the La–Zr co-doped TiO_2 under UV light irradiation can be ascribed to simultaneous effects of La and Zr ions, which act as electron traps and enhanced adsorption of 4-NP on La–Zr co-doped TiO_2 surface.

Acknowledgement

The authors are grateful to the Research Council of Guilan University for the partial support of this study.

References

[1] G. Pfaff, P. Reynders, Angle-dependent optical effects deriving from submicron structures of films and pigments, Chem. Rev. 99 (1999) 1963–1981.
[2] Y.C. Yeh, T.T. Tseng, D.A. Chang, Electrical properties of porous titania ceramic humidity sensors, J. Am. Ceram. Soc. 72 (1989) 1472–1475.
[3] P.S. Awati, S.V. Awate, P.P. Shah, V. Ramaswamy, Photocatalytic decomposition of methylene blue using nanocrystalline anatase titania prepared by ultrasonic technique, Catal. Commun. 4 (2003) 393–400.
[4] A. Hagfeldt, M. Gratzel, Light-induced redox reactions in nanocrystalline systems, Chem. Rev. 95 (1995) 49–68.
[5] M.V. Rao, K. Rajeshwar, V.R. Pai Verneker, J. DuBow, Photosyntlhetic production of H_2 and H_2O_2 on semiconducting oxide grains in aqueous solutions, J. Phys. Chem. 84 (1980) 1987–1991.
[6] A. Tsevis, N. Spanos, P.G. Koutsoukos, A.J. Linde, J. Lykleme, Preparation and characterization of anatase powders, J. Chem. Soc., Faraday Trans. 94 (1998) 295–300.
[7] S.D. Mo, L.B. Lin, Electron states of iron group impurities in doped rutile (TiO_2), J. Phys. Chem. Solids 55 (1994) 1309–1313.
[8] K. Vinodgopal, D.E. Wynkoop, P.V. Kamat, Environmental photochemistry on semiconductor surfaces: photosensitized degradation of a textile azo dye, acid orange 7, on TiO_2 particles using visible light, Environ. Sci. Technol. 30 (1996) 1660–1666.
[9] V. Vamathevan, R. Amal, D. Beydoun, G. Low, S. McEvoy, Photocatalytic oxidation of organics in water using pure and silver-modified titanium dioxide particles, J. Photochem. Photobiol. A 148 (2002) 233–245.
[10] A. Scolan, C. Sanchez, Synthesis and characterization of surface-protected nanocrystalline titania particles, Chem. Mater. 10 (1998) 3217–3223.
[11] M. Wu, J. Long, A. Huang, Y. Luo, S. Feng, R. Xu, Microemulsion-mediated hydrothermal synthesis and characterization of nanosize rutile and anatase particles, Langmuir 15 (1999) 8822–8825.
[12] M. Wu, G. Lin, D. Chen, G. Wang, D. He, S. Feng, R. Xu, Sol-hydrothermal synthesis and hydrothermally structural evolution of nanocrystal titanium dioxide, Chem. Mater. 14 (2002) 1974–1980.
[13] S. Yang, L. Gao, Preparation of titanium dioxide nanocrystallite with high photocatalytic activities, J. Am. Ceram. Soc. 88 (2005) 968–970.
[14] H.Y. Zhu, Y. Lan, X.P. Gao, S.P. Ringer, Z.F. Zheng, D.Y. Song, J.C. Zhao, Phase transition between nanostructures of titanate and titanium dioxides via simple wet-chemical reactions, J. Am. Chem. Soc. 127 (2005) 6730–6736.
[15] G. Colon, M.C. Hidalgo, J.A. Navio, A novel preparation of high surface area TiO_2 nanoparticles from alkoxide precursor and using active carbon as additive, Catal. Today 76 (2002) 91–101.
[16] K.N. Ramakrishnan, Powder particle size relationship in microwave synthesized ceramic powders, Mater. Sci. Eng. A 259 (1999) 120–125.
[17] J.A. Aylloĭn, A.M. Peiroĭ, L. Saadoun, E. Vigil, X. Dome'nech, J. Peral, Preparation of anatase powders from fluorine-complexed titanium (IV) aqueous solution using microwave irradiation, J. Mater. Chem. 10 (2000) 1911–1914.
[18] S. Komarneni, R.K. Rajha, H. Katsuki, microwave-hydrothermal processing of titanium dioxide, Mater. Chem. Phys. 61 (1999) 50–54.
[19] Z.L. Wang, Y. Liu, Z. Zhang, Handbook of Nanophase and Nanostructured Materials—Materials Systems and Applications (I), Tsinghua University Press, Beijing, 2002, pp. 74–80.
[20] F. Li, X. Li, M. Hou, Photocatalytic degradation of 2-mercaptobenzothiazole in aqueous La^{3+}–TiO_2 suspension for odor control, Appl. Catal. B: Environ. 48 (2004) 185–194.
[21] An-Wu Xu, Yuan Gao, Han-Qin Liu, The preparation, characterization, and their photocatalytic activities of rare-earth-doped TiO_2 nanoparticles, J. Catal. 207 (2002) 151–157.
[22] J. Nair, P. Nair, F. Mizukami, Y. Oosawa, T. Okubo, Microstructure and phase transformation behavior of doped nanostructured titania, Mater. Res. Bull. 34 (1999) 1275–1290.
[23] Y.H. Hsien, C.F. Chang, Y.H. Chen, S. Cheng, Photodegradation of aromatic pollutants in water over TiO_2 supported on molecular sieves, Appl. Catal. B: Environ. 31 (2001) 241–249.
[24] T. Ohsaka, F. Izumi, Y. Fujiki, Raman spectrum of anatase, TiO_2, J. Raman Spectra 6 (1978) 321–324.
[25] S.S. Chan, I.E. Wachs, L.L. Murrell, L. Wang, W.K. Hall, In situ laser Raman spectroscopy of supported metal oxides, J. Phys. Chem. 88 (1984) 5831–5835.
[26] S. Sakthivel, M.V. Shankar, M. Palanichamy, B. Arabindoo, D.W. Bahnemann, V. Murugesan, Enhancement of photocatalytic activity by metal deposition: characterisation and photonic efficiency of Pt, Au and Pd deposited on TiO_2 catalyst, Water Res. 38 (2004) 3001–3008.
[27] K. Nagaveni, M.S. Hegde, G. Madras, Structure and photocatalytic activity of $Ti_{1-x}M_xO_{2\pm\delta}$ (M = W, V, Ce, Zr, Fe, and Cu) synthesized by solution combustion method, J. Phys. Chem. B 108 (2004) 20204–20212.
[28] D. Dvoranová, V. Brezová, M. Mazúr, M.A. Malati, Investigations of metal-doped titanium dioxide photocatalysts, Appl. Catal. B: Environ. 37 (2002) 91–105.